

95 GeV Higgs boson and nano-Hertz gravitational waves from domain walls in the N2HDM

Haotian Xu, Yufei Wang, Xiao-Fang Han, Lei Wang

¹*Department of Physics, Yantai University, Yantai, Shandong 264005, China*

Abstract

We explore the diphoton and $b\bar{b}$ excesses at 95.4 GeV, as well as nano-Hertz gravitational waves originating from domain walls, within the framework of the next-to-two-Higgs-doublet model (N2HDM), which extends the two-Higgs-doublet model by introducing a real singlet scalar subject to a discrete Z_2 symmetry. The Z_2 symmetry is spontaneously broken by the non-zero vacuum expectation value of the singlet scalar, v_s , which leads to the formation of domain walls. We discuss two different scenarios: in scenario A, the 95.4 GeV Higgs boson predominantly originates from the singlet field, while in scenario B, it arises mainly from the CP-even components of the Higgs doublets. Taking into account relevant theoretical and experimental constraints, we find that scenario A can fully account for both the diphoton and $b\bar{b}$ excesses at 95.4 GeV within the 1σ range. Moreover, the peak amplitude of the gravitational wave spectrum at a peak frequency of 10^{-9} Hz can reach 2×10^{-12} for $v_s = 100$ TeV. Scenario B only marginally accounts for the diphoton and $b\bar{b}$ excesses at the 1σ level, but the peak amplitude of the gravitational wave spectrum at the peak frequency of 10^{-9} Hz can reach 6×10^{-8} for $v_s = 100$ TeV. The nano-Hertz gravitational wave spectrum predicted in both scenarios can be tested by the current and future pulsar timing array projects.

I. INTRODUCTION

The possibility of additional Higgs states beyond the Standard Model (SM) is an open question. The emergence of experimental anomalies hinting at a scalar resonance around 95.4 GeV has generated significant interest within the high-energy physics community. Hints of a light scalar near 95.4 GeV first appeared in searches at LEP collider, where a 2.3σ excess in the $e^+e^- \rightarrow Z\phi$ process with $\phi \rightarrow b\bar{b}$ was reported [1]. Recently, the CMS collaboration has observed a local significance of 2.9σ in the diphoton invariant mass spectrum around 95.4 GeV using full Run 2 data set of LHC [2]. The ATLAS experiment has also observed an excess in the diphoton channel, albeit with a lower significance [3]. Neglecting possible correlations, the combined signal strength of ATLAS and CMS has a 3.1σ local excess in the diphoton channel around 95.4 GeV [4]. There are numerous explanations on the excesses in the new physics models, for example Refs. [4–62].

On the other hand, current observations from several pulsar timing array (PTA) collaborations have yielded strong statistical evidence for a stochastic gravitational wave background (SGWB) in the nano-Hertz regime, including NANOGrav [63, 64], the European Pulsar Timing Array (EPTA) [65, 66], the Parkes Pulsar Timing Array (PPTA) [67], and the Chinese Pulsar Timing Array (CPTA) [68]. In addition to the supermassive black hole binaries interpretation [69], there are various cosmological sources of the gravitational waves (GWs), such as cosmic strings [70–80], domain walls [81–93], primordial first-order phase transitions [94–114], and inflation [115–124].

In this paper, we explore the possibility of simultaneously explaining the observed excess of 95.4 GeV Higgs boson and the nano-Hertz SGWB within the framework of the two-Higgs-doublet model extended by a real singlet scalar, commonly referred to as the N2HDM [6–8, 125–127]. In this model, the 95.4 GeV Higgs boson arises from the mixing among three CP-even scalar fields, including the singlet field. In addition, the N2HDM respects a discrete Z_2 symmetry, which is spontaneously broken by the non-zero vacuum expectation value (VEV) of the singlet scalar. The spontaneous breaking of this discrete Z_2 symmetry in the early Universe leads to the formation of domain walls that separate regions of distinct vacua. The authors of [128] studied the possibility of restoring the electroweak symmetry in the N2HDM via the domain walls. To ensure that the domain walls are unstable and eventually annihilate, the discrete symmetry is explicitly broken by introducing a very small

bias term. The peak frequency of GWs produced by the domain walls is set by the time of annihilation, while the amplitude depends on the energy density of domain wall. This model has the potential to generate domain walls whose dynamics may produce GWs in the nano-Hertz frequency band, offering a possible explanation for the signals observed by PTA experiments.

The remainder of this paper is organized as follows. In Section II we present the key features of the N2HDM. In Sections III and IV, we examine the relevant theoretical and experimental constraints, and discuss the explanation of the diphoton and $b\bar{b}$ excesses at 95.4 GeV. In Section V we explore the domain walls and the associated GW spectra. Finally, we summarize our conclusions in Section VI.

II. THE MODEL

The two-Higgs-doublet model is extended by introducing a real singlet scalar,

$$\Phi_1 = \begin{pmatrix} \phi_1^+ \\ \frac{(v_1 + \rho_1 + i\eta_1)}{\sqrt{2}} \end{pmatrix}, \Phi_2 = \begin{pmatrix} \phi_2^+ \\ \frac{(v_2 + \rho_2 + i\eta_2)}{\sqrt{2}} \end{pmatrix}, \Phi_S = \rho_s + v_s, \quad (1)$$

After spontaneous symmetry breaking, the fields Φ_1 , Φ_2 and Φ_S acquire their VEVs v_1 , v_2 , and v_s , with $v \equiv \sqrt{v_1^2 + v_2^2} = 246$ GeV. The ratio of the two-Higgs-doublet VEVs is defined as $\tan \beta \equiv v_2/v_1$.

The Higgs potential is written as

$$\begin{aligned} V = & m_{11}^2 |\Phi_1|^2 + m_{22}^2 |\Phi_2|^2 - m_{12}^2 (\Phi_1^\dagger \Phi_2 + \text{h.c.}) + \frac{\lambda_1}{2} (\Phi_1^\dagger \Phi_1)^2 + \frac{\lambda_2}{2} (\Phi_2^\dagger \Phi_2)^2 \\ & + \lambda_3 (\Phi_1^\dagger \Phi_1) (\Phi_2^\dagger \Phi_2) + \lambda_4 (\Phi_1^\dagger \Phi_2) (\Phi_2^\dagger \Phi_1) + \frac{\lambda_5}{2} [(\Phi_1^\dagger \Phi_2)^2 + \text{h.c.}] \\ & + \frac{m_S^2}{2} \Phi_S^2 + \frac{\lambda_6}{8} \Phi_S^4 + \frac{\lambda_7}{2} (\Phi_1^\dagger \Phi_1) \Phi_S^2 + \frac{\lambda_8}{2} (\Phi_2^\dagger \Phi_2) \Phi_S^2. \end{aligned} \quad (2)$$

We assume that the model conserves CP-symmetry, meaning all coupling constants and mass parameters to be real. The Higgs potential in Eq. (2) respects a discrete Z_2 symmetry,

$$\Phi_1 \rightarrow \Phi_1, \quad \Phi_2 \rightarrow \Phi_2, \quad \Phi_S \rightarrow -\Phi_S, \quad (3)$$

which is spontaneously broken by the VEV of Φ_S , giving rise to domain walls in the early

Universe. The conditions for minimizing the scalar potential lead to

$$v_2 m_{12}^2 - v_1 m_{11}^2 = \frac{1}{2}(v_1^3 \lambda_1 + v_2^2 v_1 \lambda_{345} + v_s^2 v_1 \lambda_7), \quad (4)$$

$$v_1 m_{12}^2 - v_2 m_{22}^2 = \frac{1}{2}(v_1^2 v_2 \lambda_{345} + v_2^3 \lambda_2 + v_s^2 v_2 \lambda_8), \quad (5)$$

$$-v_s m_S^2 = \frac{1}{2}v_s(v_1^2 \lambda_7 + v_2^2 \lambda_8 + v_s^2 \lambda_6), \quad (6)$$

where $\lambda_{345} \equiv \lambda_3 + \lambda_4 + \lambda_5$.

It is necessary to introduce an energy bias in the potential, which lifts the degenerate minima connected by the discrete Z_2 symmetry. This bias destabilizes the domain walls, thereby evading the associated cosmological constraints [129–131]. Here we introduce the Z_2 symmetry-breaking potential term by hand,

$$V_{Z_2} = -a_1 v_s^2 \Phi_S + \frac{a_1}{3} \Phi_S^3. \quad (7)$$

The total potential still has minima at $(v_1, v_2, \pm v_s)$, but there is an energy difference between them

$$V_{\text{bias}} = V(v_1, v_2, -v_s) - V(v_1, v_2, v_s) = \frac{4}{3} a_1 v_s^3. \quad (8)$$

In fact, since the required values of a_1 is extremely small, we only consider it in the discussions of domain walls, and neglect it in other calculations.

Once spontaneous symmetry breaking occurs, the mass eigenstates are derived from the original fields through the application of rotation matrices

$$\begin{pmatrix} h_1, h_2, h_3 \end{pmatrix} = \begin{pmatrix} \rho_1, \rho_2, \rho_s \end{pmatrix} R^T, \quad (9)$$

$$\begin{pmatrix} G^0 \\ A \end{pmatrix} = \begin{pmatrix} \cos \beta & \sin \beta \\ -\sin \beta & \cos \beta \end{pmatrix} \begin{pmatrix} \eta_1 \\ \eta_2 \end{pmatrix}, \quad (10)$$

$$\begin{pmatrix} G^\pm \\ H^\pm \end{pmatrix} = \begin{pmatrix} \cos \beta & \sin \beta \\ -\sin \beta & \cos \beta \end{pmatrix} \begin{pmatrix} \phi_1^\pm \\ \phi_2^\pm \end{pmatrix}, \quad (11)$$

with

$$R = \begin{pmatrix} c_1 c_2 & s_1 c_2 & s_2 \\ -s_1 c_3 - c_1 s_2 s_3 & c_1 c_3 - s_1 s_2 s_3 & c_2 s_3 \\ s_1 s_3 - c_1 s_2 c_3 & -s_1 s_2 c_3 - c_1 s_3 & c_2 c_3 \end{pmatrix}. \quad (12)$$

The shorthand notations are $s_{1,2,3} \equiv \sin \alpha_{1,2,3}$ and $c_{1,2,3} \equiv \cos \alpha_{1,2,3}$. The G^0 and G^\pm correspond to the Goldstone bosons, which are absorbed by the Z and W^\pm . The remaining

physical states consist of three CP-even scalars $h_{1,2,3}$, one pseudoscalars A , and a pair of charged scalar H^\pm .

The coupling constants in the Higgs potential can be expressed in terms of the scalar masses and mixing angles as

$$\begin{aligned}
\lambda_1 &= \frac{m_{h_1}^2 R_{11}^2 + m_{h_2}^2 R_{21}^2 + m_{h_3}^2 R_{31}^2 - m_{12}^2 t_\beta}{v^2 c_\beta^2}, \\
\lambda_2 &= \frac{m_{h_1}^2 R_{12}^2 + m_{h_2}^2 R_{22}^2 + m_{h_3}^2 R_{32}^2 - m_{12}^2 t_\beta^{-1}}{v^2 s_\beta^2}, \\
\lambda_3 &= \frac{m_{h_1}^2 R_{11}R_{12} + m_{h_2}^2 R_{21}R_{22} + m_{h_3}^2 R_{31}R_{32} + 2m_{H^\pm}^2 s_\beta c_\beta - m_{12}^2}{v^2 s_\beta c_\beta}, \\
\lambda_4 &= \frac{(m_A^2 - 2m_{H^\pm}^2) s_\beta c_\beta + m_{12}^2}{v^2 s_\beta c_\beta}, \\
\lambda_5 &= \frac{-m_A^2 s_\beta c_\beta + m_{12}^2}{v^2 s_\beta c_\beta}, \\
\lambda_6 &= \frac{m_{h_1}^2 R_{13}^2 + m_{h_2}^2 R_{23}^2 + m_{h_3}^2 R_{33}^2 - 2a_1 v_s}{v_s^2}, \\
\lambda_7 &= \frac{m_{h_1}^2 R_{11}R_{13} + m_{h_2}^2 R_{21}R_{23} + m_{h_3}^2 R_{31}R_{33}}{v v_s c_\beta}, \\
\lambda_8 &= \frac{m_{h_1}^2 R_{12}R_{13} + m_{h_2}^2 R_{22}R_{23} + m_{h_3}^2 R_{32}R_{33}}{v v_s s_\beta},
\end{aligned} \tag{13}$$

with shorthand notation $t_\beta \equiv \tan \beta$.

In order to avoid the flavour changing neutral current at the tree-level, one imposes a \mathbb{Z}'_2 symmetry (see, e.g., the recent review [132]),

$$u_R \rightarrow -u_R, \quad d_R \rightarrow -d_R, \quad e_R \rightarrow -e_R, \quad \Phi_2 \rightarrow -\Phi_2, \tag{14}$$

while the other fields remain unchanged. This results in the well-known type-I Yukawa interactions,

$$-\mathcal{L} = Y_{u2} \bar{Q}_L \tilde{\Phi}_2 u_R + Y_{d2} \bar{Q}_L \Phi_2 d_R + Y_{e2} \bar{L}_L \Phi_2 e_R + \text{h.c.} \tag{15}$$

Where $Q_L^T = (u_L, d_L)$, $L_L^T = (\nu_L, l_L)$, $\tilde{\Phi}_2 = i\tau_2 \Phi_2^*$, and Y_{u2} , Y_{d2} and Y_{e2} are 3×3 matrices in family space. However, the \mathbb{Z}'_2 symmetry is explicitly broken in the scalar potential of Eq. (2).

The neutral Higgs boson couplings, normalized to the SM values, are given by

$$\begin{aligned}
y_V^{h_1} &= c_2 c_{\beta_1}, \quad y_f^{h_1} = c_2 (c_{\beta_1} - s_{\beta_1} \kappa_f), \\
y_V^{h_2} &= c_3 s_{\beta_1} - s_2 s_3 c_{\beta_1}, \quad y_f^{h_2} = c_3 (s_{\beta_1} + c_{\beta_1} \kappa_f) - s_2 s_3 (c_{\beta_1} - s_{\beta_1} \kappa_f), \\
y_V^{h_3} &= -s_3 s_{\beta_1} - s_2 c_3 c_{\beta_1}, \quad y_f^{h_3} = -s_3 (s_{\beta_1} + c_{\beta_1} \kappa_f) - s_2 c_3 (c_{\beta_1} - s_{\beta_1} \kappa_f), \\
y_V^A &= 0, \quad y_f^A = -i\kappa_f \text{ (for } u), \quad y_f^A = i\kappa_f \text{ (for } d, \ell).
\end{aligned} \tag{16}$$

Here $\kappa_f = 1/\tan\beta$ and V stands for Z or W . The shorthand notations are defined as $c_{\beta_1} \equiv \cos(\beta - \alpha_1)$ and $s_{\beta_1} \equiv \sin(\beta - \alpha_1)$.

The charged Higgs Yukawa couplings are given by

$$\mathcal{L}_Y = -\frac{\sqrt{2}}{v} H^+ \left\{ \bar{u}_i [\kappa_f (V_{CKM})_{ij} m_{d_j} P_R - \kappa_f m_{u_i} (V_{CKM})_{ij} P_L] d_j + \kappa_f \bar{\nu} m_\ell P_R \ell \right\} + h.c., \tag{17}$$

where $i, j = 1, 2, 3$ are the index of generation.

III. RELEVANT THEORETICAL AND EXPERIMENTAL CONSTRAINTS

In our discussions, we take into account the following theoretical and experimental constraints:

(1) Vacuum stability. The following conditions are required by the vacuum stability [126],

$$\Omega_1 \text{ or } \Omega_2 \tag{18}$$

with

$$\begin{aligned}
\Omega_1 &= \left\{ \lambda_1, \lambda_2, \lambda_6 > 0; \sqrt{\lambda_1 \lambda_6} + \lambda_7 > 0; \sqrt{\lambda_2 \lambda_6} + \lambda_8 > 0; \right. \\
&\quad \left. \sqrt{\lambda_1 \lambda_2} + \lambda_3 + D > 0; \lambda_7 + \sqrt{\frac{\lambda_1}{\lambda_2}} \lambda_8 \geq 0 \right\}, \\
\Omega_2 &= \left\{ \lambda_1, \lambda_2, \lambda_6 > 0; \sqrt{\lambda_2 \lambda_6} \geq \lambda_8 > -\sqrt{\lambda_2 \lambda_6}; \sqrt{\lambda_1 \lambda_6} > -\lambda_7 \geq \sqrt{\frac{\lambda_1}{\lambda_2}} \lambda_8; \right. \\
&\quad \left. \sqrt{(\lambda_7^2 - \lambda_1 \lambda_6)(\lambda_8^2 - \lambda_2 \lambda_6)} > \lambda_7 \lambda_8 - (D + \lambda_3) \lambda_6 \right\}.
\end{aligned} \tag{19}$$

Here $D = \min(\lambda_4 - |\lambda_5|, 0)$.

(2) Tree-level perturbative unitarity. The eigenvalues of the $2 \rightarrow 2$ scalar-scalar scattering matrix are below 8π , which are [126]

$$\begin{aligned}
|\lambda_3 - \lambda_4| &< 8\pi \\
|\lambda_3 + 2\lambda_4 \pm 3\lambda_5| &< 8\pi \\
\left| \frac{1}{2} \left(\lambda_1 + \lambda_2 + \sqrt{(\lambda_1 - \lambda_2)^2 + 4\lambda_4^2} \right) \right| &< 8\pi \\
\left| \frac{1}{2} \left(\lambda_1 + \lambda_2 + \sqrt{(\lambda_1 - \lambda_2)^2 + 4\lambda_5^2} \right) \right| &< 8\pi \\
|\lambda_7|, |\lambda_8| &< 8\pi, \\
\frac{1}{2}|a_{1,2,3}| &< 8\pi,
\end{aligned} \tag{20}$$

where $a_{1,2,3}$ are the real roots of the cubic equation,

$$\begin{aligned}
&4 \left(-27\lambda_1\lambda_2\lambda_6 + 12\lambda_3^2\lambda_6 + 12\lambda_3\lambda_4\lambda_6 + 3\lambda_4^2\lambda_6 + 6\lambda_2\lambda_7^2 - 8\lambda_3\lambda_7\lambda_8 - 4\lambda_4\lambda_7\lambda_8 + 6\lambda_1\lambda_8^2 \right) \\
&+ x \left(36\lambda_1\lambda_2 - 16\lambda_3^2 - 16\lambda_3\lambda_4 - 4\lambda_4^2 + 18\lambda_1\lambda_6 + 18\lambda_2\lambda_6 - 4\lambda_7^2 - 4\lambda_8^2 \right) \\
&+ x^2 \left(-6(\lambda_1 + \lambda_2) - 3\lambda_6 \right) + x^3.
\end{aligned} \tag{21}$$

(3) The 125 GeV Higgs signal data. We identify h_2 as the observed 125 GeV Higgs boson and use `HiggsTools` [133] to compute the total χ_{125}^2 based on the latest LHC measurements of signal strength of the 125 GeV Higgs boson. `HiggsTools` integrates both `HiggsSignals` [133, 134] and `HiggsBounds` [135, 136]. In particular, we focus on the parameter points that satisfy $\chi_{125}^2 - \chi_{SM}^2 < 6.18$, where χ_{SM}^2 stands for the SM prediction value. These points are preferred over the SM at the 2σ confidence level, assuming a two-parameter fit.

(4) Searches for additional Higgs boson at the collider and flavor observables. We utilize `Higgstools` to retain only those parameter points that are consistent with the 95% confidence level exclusion limits from collider searches for additional Higgs bosons. We employ `SuperIso-v4.1` [137] to assess the bound of $B \rightarrow X_s\gamma$ decay.

(5) The oblique parameters. The oblique parameters provide important constraints on the Higgs mass spectrum within the model. To ensure consistency with experimental data, parameter points are required to lie within the 2σ confidence region for both the S and T parameters. This corresponds to $\chi^2 < 6.18$ for two degrees of freedom. The corresponding fit results can be found in Ref. [138],

$$S = 0.00 \pm 0.07, \quad T = 0.05 \pm 0.06, \tag{22}$$

with a correlation coefficient $\rho_{ST} = 0.92$.

In the model, the approximate calculations of the S and T parameters are [139, 140]

$$\begin{aligned}
S &= \frac{1}{\pi m_Z^2} \left[\sum_{i=1,2,3} (F_S(m_Z^2, m_{h_i}^2, m_A^2)(-s_\beta R_{i1} + c_\beta R_{i2})^2 \right. \\
&\quad + F_S(m_Z^2, m_Z^2, m_{h_i}^2)(c_\beta R_{i1} + s_\beta R_{i2})^2 - m_Z^2 F_{S0}(m_Z^2, m_Z^2, m_{h_i}^2)(c_\beta R_{i1} + s_\beta R_{i2})^2) \\
&\quad \left. - F_S(m_Z^2, m_{H^\pm}^2, m_{H^\pm}^2) - F_S(m_Z^2, m_Z^2, m_{ref}^2) + m_Z^2 F_{S0}(m_Z^2, m_Z^2, m_{ref}^2) \right], \\
T &= \frac{1}{16\pi m_W^2 s_W^2} \left[\sum_{i=1,2,3} (-F_T(m_{h_i}^2, m_A^2)(-s_\beta R_{i1} + c_\beta R_{i2})^2 \right. \\
&\quad + F_T(m_{H^\pm}^2, m_{h_i}^2)(c_\beta R_{i2} - s_\beta R_{i1})^2 \\
&\quad + 3F_T(m_Z^2, m_{h_i}^2)(c_\beta R_{i1} + s_\beta R_{i2})^2 - 3F_T(m_W^2, m_{h_i}^2)(c_\beta R_{i1} + s_\beta R_{i2})^2) \\
&\quad \left. + F_T(m_{H^\pm}^2, m_A^2) - 3F_T(m_Z^2, m_{ref}^2) + 3F_T(m_W^2, m_{ref}^2) \right], \tag{23}
\end{aligned}$$

with

$$\begin{aligned}
F_T(a, b) &= \frac{1}{2}(a + b) - \frac{ab}{a - b} \log\left(\frac{a}{b}\right), \quad F_S(a, b, c) = B_{22}(a, b, c) - B_{22}(0, b, c), \\
F_{S0}(a, b, c) &= B_0(a, b, c) - B_0(0, b, c) \tag{24}
\end{aligned}$$

where

$$\begin{aligned}
B_{22}(a, b, c) &= \frac{1}{4} \left[b + c - \frac{1}{3}a \right] - \frac{1}{2} \int_0^1 dx X \log(X - i\epsilon), \\
B_0(a, b, c) &= - \int_0^1 dx \log(X - i\epsilon), \\
X &= bx + c(1 - x) - ax(1 - x). \tag{25}
\end{aligned}$$

IV. THE DIPHOTON AND $b\bar{b}$ EXCESSES AT 95.4 GEV

The combined analysis of ATLAS and CMS diphoton data at 95.4 GeV reveals a 3.1σ local excess [4].

$$\mu_{\gamma\gamma}^{exp} = \mu_{\gamma\gamma}^{ATLAS+CMS} = 0.24_{-0.08}^{+0.09}. \tag{26}$$

Intriguingly, a persistent local excess with a significance of 2.3σ was also observed in the $e^+e^- \rightarrow Z(\phi \rightarrow b\bar{b})$ channel at LEP in the same mass region [1],

$$\mu_{b\bar{b}}^{exp} = 0.117 \pm 0.057. \tag{27}$$

The observed excesses in the diphoton and $b\bar{b}$ channels at 95.4 GeV are attributed to resonant production of the lightest CP-even Higgs boson, h_1 . Under the narrow width approximation, the corresponding signal strengths can be formulated as follows:

$$\mu_{b\bar{b}} = \frac{\sigma_{\text{N2HDM}}(e^+e^- \rightarrow Zh_1)}{\sigma_{\text{SM}}(e^+e^- \rightarrow Zh_{95.4}^{\text{SM}})} \times \frac{\text{BR}_{\text{N2HDM}}(h_1 \rightarrow b\bar{b})}{\text{BR}_{\text{SM}}(h_{95.4}^{\text{SM}} \rightarrow b\bar{b})} = |y_V^{h_1}|^2 \frac{\text{BR}_{\text{N2HDM}}(h_1 \rightarrow b\bar{b})}{\text{BR}_{\text{SM}}(h_{95.4}^{\text{SM}} \rightarrow b\bar{b})}, \quad (28)$$

$$\mu_{\gamma\gamma} = \frac{\sigma_{\text{N2HDM}}(gg \rightarrow h_1)}{\sigma_{\text{SM}}(gg \rightarrow h_{95.4}^{\text{SM}})} \times \frac{\text{BR}_{\text{N2HDM}}(h_1 \rightarrow \gamma\gamma)}{\text{BR}_{\text{SM}}(h_{95.4}^{\text{SM}} \rightarrow \gamma\gamma)} \simeq |y_f^{h_1}|^2 \frac{\text{BR}_{\text{N2HDM}}(h_1 \rightarrow \gamma\gamma)}{\text{BR}_{\text{SM}}(h_{95.4}^{\text{SM}} \rightarrow \gamma\gamma)}. \quad (29)$$

To assess the capability to simultaneously account for the observed excesses in the $\gamma\gamma$ and $b\bar{b}$ channels, we conduct a χ_{95}^2 analysis,

$$\chi_{95}^2 = \frac{(\mu_{\gamma\gamma} - 0.24)^2}{0.085^2} + \frac{(\mu_{b\bar{b}} - 0.117)^2}{0.057^2}, \quad (30)$$

and explain the diphoton and $b\bar{b}$ excesses within the 2σ ranges, namely $\chi_{95}^2 < 6.18$.

In the model, the decay $h_1 \rightarrow \gamma\gamma$ is induced at the one-loop level, whose width is calculated as

$$\Gamma(h_1 \rightarrow \gamma\gamma) = \frac{\alpha^2 m_{h_1}^3}{256\pi^3 v^2} \left| y_V^{h_1} F_1(\tau_{W^\pm}) + y_{H^\pm} F_0(\tau_{H^\pm}) + \sum_f y_f^{h_1} N_{cf} Q_f^2 F_{1/2}(\tau_f) \right|^2, \quad (31)$$

where $\tau_i = \frac{4m_i^2}{m_{h_1}^2}$, and N_{cf} and Q_f are electric charge and the number of color degrees of freedom of the fermion in the loop. The factor y_{H^\pm} is

$$y_{H^\pm} = \frac{v}{2m_{h^\pm}^2} g_{h_1 H^+ H^-} \quad (32)$$

with

$$g_{h_1 H^+ H^-} = \frac{1}{v} \left(-\frac{m_{12}^2}{s_\beta c_\beta} \left[\frac{R_{11}}{c_\beta} + \frac{R_{12}}{s_\beta} \right] + m_{h_1}^2 \left[\frac{R_{11} s_\beta^2}{c_\beta} + \frac{R_{12} c_\beta^2}{s_\beta} \right] + 2m_{H^\pm}^2 [R_{11} c_\beta + R_{12} s_\beta] \right) \quad (33)$$

The functions $F_{1,0,1/2}$ are defined as [141]

$$F_1(\tau) = 2 + 3\tau + 3\tau(2-\tau)f(\tau), \quad F_{1/2}(\tau) = -2\tau[1 + (1-\tau)f(\tau)], \quad F_0(\tau) = \tau[1 - \tau f(\tau)], \quad (34)$$

with

$$f(\tau) = \begin{cases} [\sin^{-1}(1/\sqrt{\tau})]^2, & \tau \geq 1 \\ -\frac{1}{4}[\ln(\eta_+/\eta_-) - i\pi]^2, & \tau < 1 \end{cases} \quad (35)$$

where $\eta_\pm = 1 \pm \sqrt{1-\tau}$.

In our calculations, we take two different scenarios:

Scenario A: By choosing a small value of c_2 , the 95.4 GeV Higgs boson (h_1) is predominantly singlet-like, originating mainly from the singlet field Φ_S . Under the approximation of $s_2 \simeq \text{sgn}(s_2)(1 - \frac{c_2^2}{2})$, the couplings h_2 and h_3 normalized to the SM are given by

$$\begin{aligned} y_V^{h_2} &\simeq |s_2|s_{\beta 13} + \frac{c_2^2}{2}c_3s_{\beta 1}, & y_f^{h_2} &\simeq |s_2|(s_{\beta 13} + c_{\beta 13}\kappa_f) + \frac{c_2^2}{2}c_3(s_{\beta 1} + c_{\beta 1}\kappa_f), \\ y_V^{h_3} &\simeq |s_2|c_{\beta 13} - \frac{c_2^2}{2}c_3s_{\beta 1}, & y_f^{h_3} &\simeq |s_2|(c_{\beta 13} - s_{\beta 13}\kappa_f) - \frac{c_2^2}{2}c_3(s_{\beta 1} + c_{\beta 1}\kappa_f), \end{aligned} \quad (36)$$

where $c_{\beta 13} \equiv \cos(\beta - \alpha_1 - \text{sgn}(s_2)\alpha_3)$ and $s_{\beta 13} \equiv \sin(\beta - \alpha_1 - \text{sgn}(s_2)\alpha_3)$. The mixing parameters are chosen as follows:

$$0 \leq c_2 \leq 0.4, \quad s_{\beta 13} = 1.0, \quad 0 \leq c_{\beta 1} \leq 1.0, \quad 1 \leq \tan \beta \leq 15. \quad (37)$$

When $s_{\beta 13} = 1.0$ and c_2 approaches zero, the couplings of h_2 to the SM particles converge to those of the SM Higgs boson, which is favored by the observed signal data for the 125 GeV Higgs.

Scenario B: The mixing parameters are scanned over the following ranges:

$$0 \leq c_{\beta 1} \leq 0.4, \quad -0.4 \leq s_3 \leq 0.4, \quad 0 \leq c_2 \leq 1, \quad 1 \leq \tan \beta \leq 15. \quad (38)$$

In the limits of $c_{\beta 1} \rightarrow 0$ and $|s_3| \rightarrow 0$, the couplings of h_2 to the SM particles approach those of the SM, which is favored by the signal measurements of the 125 GeV Higgs. In addition, when $c_2 \rightarrow 1$, the 95.4 GeV Higgs boson (h_1) predominantly originates from the mixing of the two CP-even components of the Higgs doublets.

After imposing the relevant theoretical constraints, the oblique parameters, the Higgs signal data at 125 GeV, searches for additional Higgs bosons at the collider, and flavor observables, we identify the parameter space in scenario A that accounts for the observed excesses in the $b\bar{b}$ and diphoton channels at 95.4 GeV in Fig. 1. As indicated by Eq. (36), within the selected parameter space of scenario A, the coupling of h_2 to vector bosons, $y_V^{h_2}$, tends to be smaller than its coupling to fermions, $y_f^{h_2}$, as illustrated in the left panel. The Higgs signal data at 125 GeV impose a lower bound on $y_V^{h_2}$, requiring $y_V^{h_2} > 0.93$. In the parameter space consistent with the 125 GeV Higgs measurements, collider limits on additional Higgs bosons, and constraints from flavor physics, the coupling $y_V^{h_1}$ is restricted to values below 0.38. Furthermore, the condition $\chi_{95}^2 < 6.18$ is satisfied in the region of

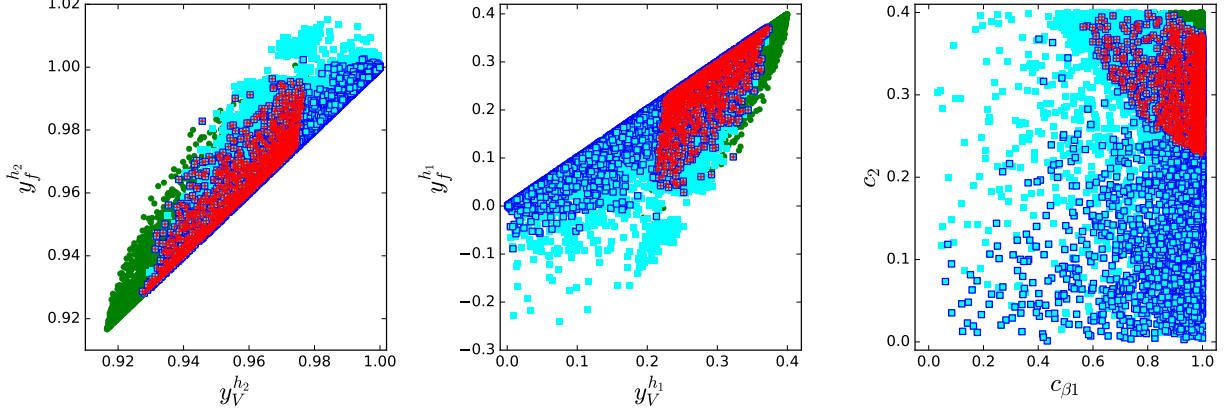


FIG. 1: In scenario A, the parameter space is progressively constrained by sequentially imposing the following: theoretical requirements and the oblique parameters; the signal data of the 125 GeV Higgs boson; searches for additional Higgs bosons at the collider and flavour observables; and finally the condition $\chi_{95}^2 < 6.18$. The surviving parameter points at each stage are represented by green bullets, cyan squares, blue-edged squares, and red pluses, respectively.

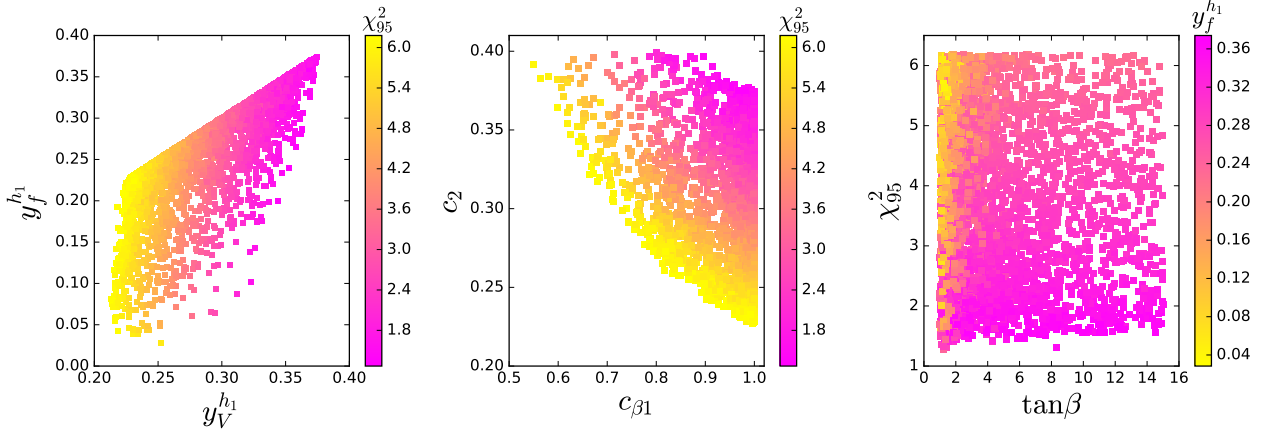


FIG. 2: In scenario A, the surviving parameter points satisfy $\chi_{95}^2 < 6.18$ while remaining consistent with the theoretical constraints, the oblique parameters, the Higgs signal data at 125 GeV, searches for additional Higgs bosons at the collider, and flavor observables.

$0.2 \leq y_V^{h1} \leq 0.38$, with y_f^{h1} bounded from below. In addition, the Higgs signal data at 125 GeV exclude a small corner of the parameter space characterized by $c_{\beta1} \rightarrow 1$ and $c_2 \rightarrow 0.4$. In such region both y_V^{h2} and y_f^{h2} can exhibit significant deviations from unity.

As shown in the left panel of Fig. 2, the value of χ_{95}^2 is sensitive to y_V^{h1} and y_f^{h1} , and decreases as they increase. The condition $\chi_{95}^2 < 2.3$ is satisfied in partial region of parameter space, with the minimum value attaining 1.2, which indicates that the model can explain

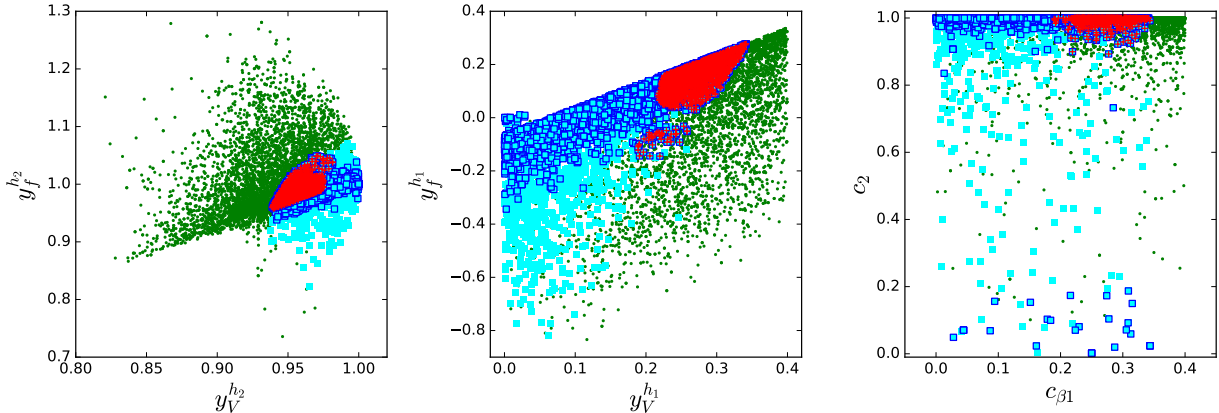


FIG. 3: Same as the Fig. 1, but for scenario B.

the diphoton and $b\bar{b}$ excesses within the 1σ ranges. The signal strength $\mu_{b\bar{b}}$ is proportional to $|y_V^{h_1}|^2$. Meanwhile, the W -loop can play an important contribution to the width of $h_1 \rightarrow \gamma\gamma$, and therefore the signal strength $\mu_{\gamma\gamma}$ is also affected by $y_V^{h_1}$. The interpretation of the $b\bar{b}$ excess imposes a lower bound on $|y_f^{h_1}|$. Because of $y_V^{h_1} = c_2 c_{\beta 1}$, the value of χ_{95}^2 tends to decrease as c_2 and $c_{\beta 1}$ increase, as shown in the middle panel of Fig. 2. When $c_{\beta 1}$ or $\tan\beta$ is large, the $y_f^{h_1}$ will have a mild dependence on $\tan\beta$ (See Eq. (16)). From the right panel of Fig. 2, it is observed that the value of χ_{95}^2 shows limited sensitivity to $\tan\beta$.

Similar to Fig. 1, we display the parameter points for scenario B that accounts for the observed excesses in the $b\bar{b}$ and diphoton channels at 95.4 GeV in Fig. 3. Unlike scenario A, the allowed region in scenario B includes not only the positive $y_f^{h_1}$ region but also a narrow band where $y_f^{h_1}$ takes negative values. The signal data of the 125 GeV Higgs boson requires a small $c_{\beta 1}$, allowing for a negative $y_f^{h_1}$, see Eq. (16). The condition $\chi_{95}^2 < 6.18$ is satisfied in the region of $0.18 < c_{\beta 1} < 0.35$ and $0.88 < c_2 < 1$. For such large c_2 , the 95.4 GeV Higgs boson mainly originates from the mixing of the two CP-even components of the Higgs doublets.

As in scenario A, the value of χ_{95}^2 in scenario B decreases as $y_V^{h_1}$ and $|y_f^{h_1}|$ (c_2 and $c_{\beta 1}$) increase, as illustrated in the upper-left panel and upper-right panel of Fig. 4. However, different from scenario A, the minimal value of χ_{95}^2 in scenario B only reaches to 2, suggesting that the model can only marginally explain the diphoton and $b\bar{b}$ excesses at the 1σ level. Furthermore, the condition $\chi_{95}^2 < 6.18$ disfavors a narrow region around $\tan\beta \sim 4$, where the value of $|y_f^{h_1}|$ is significantly suppressed. The parameter s_3 is favored to vary from -0.3 to 0.25, and is not sensitive to c_2 . Its absolute value decreases with increasing $c_{\beta 1}$ in order

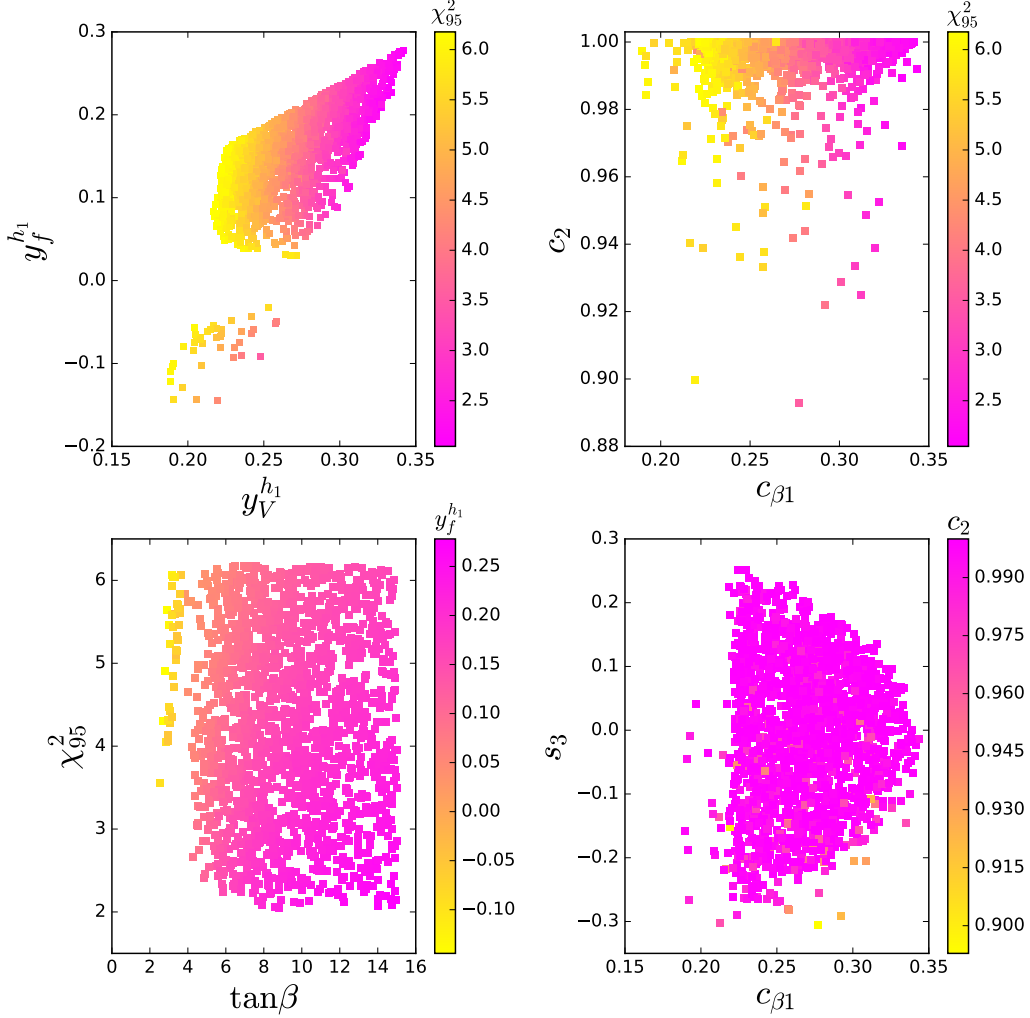


FIG. 4: Same as the Fig. 2, but for scenario B.

to maintain a sufficiently large $y_V^{h_2}$ to accommodate the signal data of the 125 GeV Higgs boson.

V. DOMAIN WALLS AND GRAVITATIONAL WAVES

The classical scalar fields are parameterized as

$$\Phi_1 = \begin{pmatrix} 0 \\ \frac{\phi_1(z)}{\sqrt{2}} \end{pmatrix}, \Phi_2 = \begin{pmatrix} 0 \\ \frac{\phi_2(z)}{\sqrt{2}} \end{pmatrix}, \Phi_S = \phi_s(z), \quad (39)$$

where z is a coordinate perpendicular to domain walls [142]. The expression for the energy density of the domain walls is given by

$$\varepsilon_{\text{wall}} = \frac{1}{2}(\partial_z \phi_1)^2 + \frac{1}{2}(\partial_z \phi_2)^2 + \frac{1}{2}(\partial_z \phi_s)^2 + V(\phi_1, \phi_2, \phi_s) - V(v_1, v_2, v_s), \quad (40)$$

with the scalar potential

$$\begin{aligned}
V(\phi_1, \phi_2, \phi_S) = & \frac{m_{11}^2}{2} \phi_1^2 + \frac{\lambda_1}{8} \phi_1^4 + \frac{m_{22}^2}{2} \phi_2^2 + \frac{\lambda_2}{8} \phi_2^4 - m_{12}^2 \phi_1 \phi_2 + \frac{\lambda_{345}}{4} \phi_1^2 \phi_2^2 \\
& + \frac{m_S^2}{2} \phi_S^2 + \frac{\lambda_6}{8} \phi_S^4 + \frac{\lambda_7}{4} \phi_1^2 \phi_S^2 + \frac{\lambda_8}{4} \phi_2^2 \phi_S^2 - a_1 v_s^2 \phi_S + \frac{a_1}{3} \phi_S^3.
\end{aligned} \tag{41}$$

The equations of motion for domain walls are

$$\frac{d^2 \phi_i}{dz^2} = \frac{\partial V(\phi_1, \phi_2, \phi_S)}{\partial \phi_i}, \quad (\phi_i = \phi_1, \phi_2, \phi_S), \tag{42}$$

with the boundary conditions

$$\lim_{z \rightarrow \pm\infty} \phi_1(z) = v_1, \quad \lim_{z \rightarrow \pm\infty} \phi_2(z) = v_2, \quad \lim_{z \rightarrow \pm\infty} \phi_S(z) = \pm v_s. \tag{43}$$

We modify `CosmoTransitions` [143] to approximately solve Eqs. (42) and (43), and relevant computational details are provided in [143, 144]. The domain wall tension σ_{wall} is computed through an integration of the energy density $\varepsilon_{\text{wall}}$ over the z axis,

$$\sigma_{\text{wall}} = \int dz \varepsilon_{\text{wall}}. \tag{44}$$

Domain walls must collapse before they can overclose the Universe. The volume pressure induced by energy bias (V_{bias}) exerts a force on the domain walls, and drives the contraction of regions occupied by the false vacuum. The collapse of domain wall occurs when the volume pressure force becomes comparable to the tension force. The characteristic temperature at which the domain walls annihilate can be estimated by [145, 146]

$$T_{\text{ann}} = 3.41 \times 10^{-2} \text{ GeV } C_{\text{ann}}^{-1/2} A^{-1/2} \left(\frac{g_*(T_{\text{ann}})}{10} \right)^{-1/4} \hat{\sigma}_{\text{wall}}^{-1/2} \hat{V}_{\text{bias}}^{1/2}, \tag{45}$$

with

$$\hat{\sigma}_{\text{wall}} \equiv \frac{\sigma_{\text{wall}}}{\text{TeV}^3}, \quad \hat{V}_{\text{bias}} \equiv \frac{V_{\text{bias}}}{\text{MeV}^4}. \tag{46}$$

In this analysis, we adopt a constant $C_{\text{ann}} = 5$ [146] and set the area parameter $A \simeq 0.8$ for the Z_2 symmetric model [145]. The energetic particles released from the collapse of domain walls have the potential to disrupt the synthesis of light nuclei formed during Big Bang Nucleosynthesis (BBN) [147]. To preserve the successful predictions of BBN, it is therefore imperative that the domain walls annihilate before the BBN epoch, $T_{\text{ann}} > T_{\text{BBN}} = 8.6 \times 10^{-3}$ GeV. In addition, in order to ensure that domain walls annihilate before their energy density dominates the Universe, a lower bound must be imposed on V_{bias} [146]

$$V_{\text{bias}}^{1/4} > 2.18 \times 10^{-5} C_{\text{ann}}^{1/4} A^{1/2} \hat{\sigma}_{\text{wall}}^{1/2}. \tag{47}$$

Following the annihilation of domain walls, a SGWB is produced, and the peak frequency is given by [145]

$$\begin{aligned} f_{\text{peak}} &\simeq 1.1 \times 10^{-7} \text{ Hz} \left(\frac{g_*(T_{\text{ann}})}{10} \right)^{1/2} \left(\frac{g_{*s}(T_{\text{ann}})}{10} \right)^{-1/3} \left(\frac{T_{\text{ann}}}{1 \text{ GeV}} \right) \\ &\simeq 3.75 \times 10^{-9} \text{ Hz} \left(\frac{g_*(T_{\text{ann}})}{10} \right)^{1/4} \left(\frac{g_{*s}(T_{\text{ann}})}{10} \right)^{-1/3} C_{\text{ann}}^{-1/2} A^{-1/2} \hat{\sigma}_{\text{wall}}^{-1/2} \hat{V}_{\text{bias}}^{1/2}. \end{aligned} \quad (48)$$

Here, $g_*(T_{\text{ann}})$ and $g_{*s}(T_{\text{ann}})$ count the relativistic degrees of freedom contributing to the energy density and the entropy density. Within the temperature range $1 \text{ MeV} \lesssim T_{\text{ann}} \lesssim 100 \text{ MeV}$, both quantities take the value 10.75 [148].

The peak amplitude of the GW spectrum at the present time is [145, 146]

$$\Omega_{\text{GW}}^{\text{peak}} h^2 = 5.3 \times 10^{-20} \tilde{\epsilon}_{\text{GW}} A^4 C_{\text{ann}}^2 \left(\frac{g_{*s}(T_{\text{ann}})}{10} \right)^{-4/3} \left(\frac{g_*(T_{\text{ann}})}{10} \right) \hat{\sigma}_{\text{wall}}^4 \hat{V}_{\text{bias}}^{-2}. \quad (49)$$

with $\tilde{\epsilon}_{\text{GW}} \simeq 0.7 \pm 0.4$ [145]. Given an arbitrary frequency f , we use [145, 149]

$$\Omega_{\text{GW}} h^2(f < f_{\text{peak}}) = \Omega_{\text{GW}}^{\text{peak}} h^2 \left(\frac{f}{f_{\text{peak}}} \right)^3, \quad (50)$$

$$\Omega_{\text{GW}} h^2(f > f_{\text{peak}}) = \Omega_{\text{GW}}^{\text{peak}} h^2 \left(\frac{f_{\text{peak}}}{f} \right). \quad (51)$$

In our discussions, we choose f_{peak} around 10^{-9} Hz to get \hat{V}_{bias} from the second line of Eq. (48) with $\hat{\sigma}_{\text{wall}}$ calculated in the parameter points accommodating the diphoton and $b\bar{b}$ excesses at 95.4 GeV. From the first line of Eq. (48), we obtain $T_{\text{ann}} \simeq 9 \text{ MeV}$ for $f_{\text{peak}} = 10^{-9} \text{ Hz}$. In Fig. 5 and Fig. 6, we display the parameter points that satisfy $\Omega_{\text{GW}}^{\text{peak}} h^2 > 10^{-15}$ and $\chi_{95}^2 < 6.18$ while remaining consistent with relevant theoretical and experimental constraints mentioned above, for scenario A and scenario B, respectively.

For a fixed f_{peak} , both \hat{V}_{bias} and $\Omega_{\text{GW}}^{\text{peak}}$ increase with σ_{wall} , as indicated by the second line of Eq. (48) and Eq. (49), and as illustrated in the upper-left and upper-right panels of Fig. 5. In scenario A, although the 95.4 GeV Higgs boson (h_1) predominantly originates from the real singlet field, it must include non-negligible components of the Higgs doublets to acquire the necessary couplings to gauge bosons and fermions, thereby accounting for the observed diphoton and $b\bar{b}$ excesses at 95.4 GeV. Thus, both R_{31} and R_{32} can not approach to zero, theoretical constraints on $\lambda_{1,2,3}$ will impose a lower bound on m_{h_3} , $m_{h_3} < 1.2 \text{ TeV}$ (see the first three lines of Eq. (13)). As a result, according to the sixth line of Eq. (13), λ_6 decreases with increasing v_s , yielding a range of $10^{-6} < \lambda_6 < 10^{-4}$ for $14 \text{ TeV} < v_s < 100$

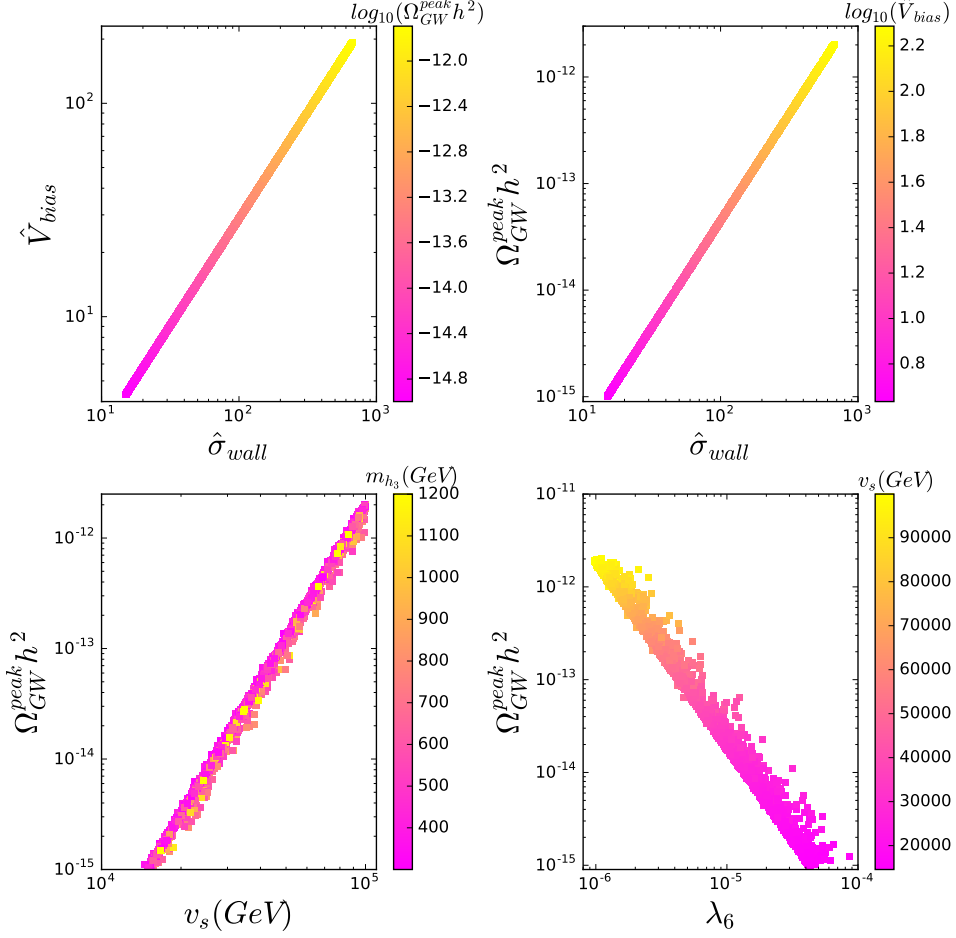


FIG. 5: In scenario A, the parameter points satisfy $\Omega_{\text{GW}}^{\text{peak}} h^2 > 10^{-15}$ and $\chi_{95}^2 < 6.18$ while remaining consistent with relevant theoretical and experimental constraints mentioned above.

TeV. As v_s increases, although λ_6 decreases, σ_{wall} still grows rapidly, resulting in $\Omega_{\text{GW}}^{\text{peak}} h^2$ reaching 2×10^{-12} for $v_s = 100$ TeV and λ_6 around 10^{-6} .

In scenario B, the 95.4 GeV Higgs boson predominantly originates from the CP-even components of the Higgs doublets. Even though the mixing between the singlet and doublet components vanishes (i.e., $R_{31} \rightarrow 0$ and $R_{32} \rightarrow 0$), the 95.4 GeV Higgs boson still can interact with gauge bosons and fermions to explain the diphoton and $b\bar{b}$ excesses at 95.4 GeV. Therefore, theoretical constraints on $\lambda_{1,2,3}$ allow m_{h_3} to have a large value, reaching up to 20 TeV in the limits $s_2 \rightarrow 0$ and $s_3 \rightarrow 0$ as illustrated in the lower-middle panel and lower-right panel of Fig. 6. As a result, λ_6 is no longer suppressed by a large v_s , and can reach 0.03 for $v_s = 100$ TeV. As shown in the Fig. 6, the peak amplitude of the GW spectrum, $\Omega_{\text{GW}}^{\text{peak}} h^2$, can reach 6×10^{-8} for $v_s = 100$ TeV, $\lambda_6 = 0.03$, $s_2 \rightarrow 0$ and $s_3 \rightarrow 0$.

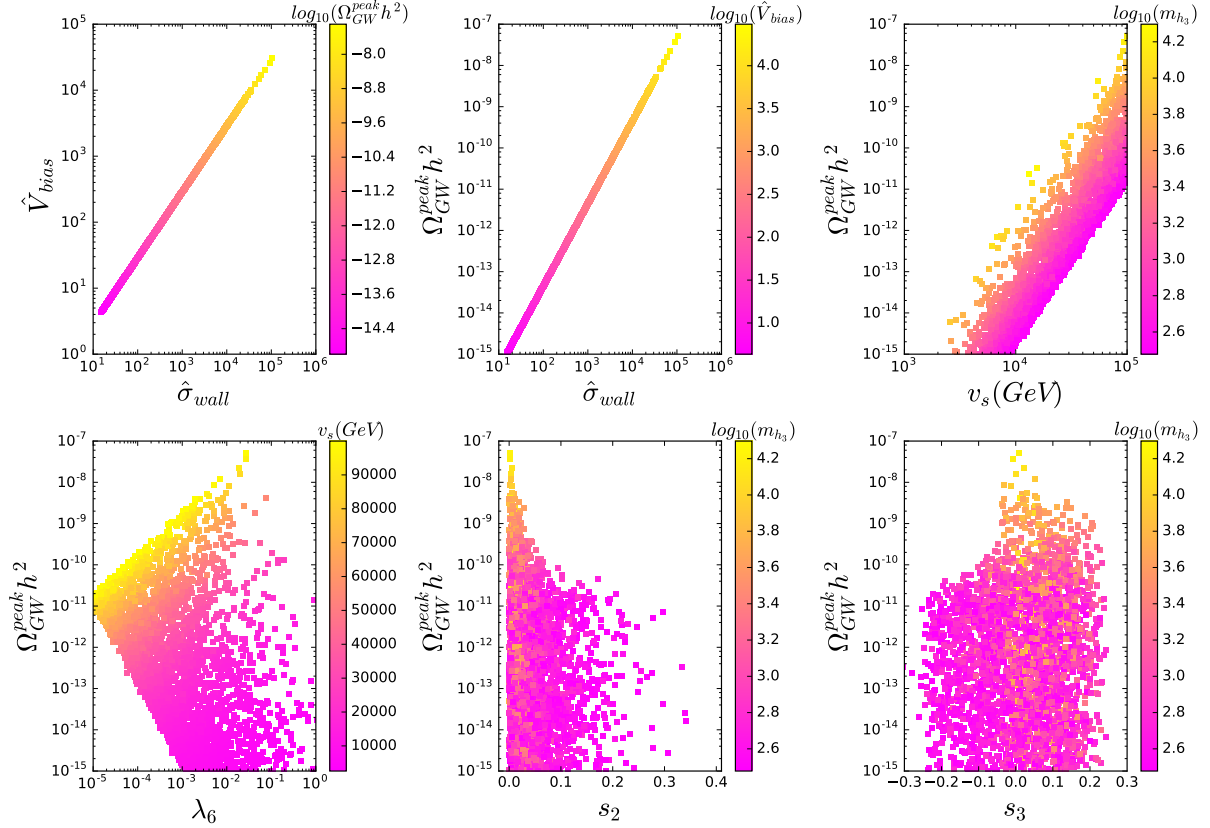


FIG. 6: Same as the Fig. 5, but for scenario B.

We pick out four benchmark points: BPA1 and BPA2 for scenario A, and BPB1 and BPB2 for scenario B, and display the key input parameters and results in Table I. We examine the GW spectra for the four benchmark points, which are shown along with the result of the NANOGrav 15-year dataset and the sensitivity curve of SKA in Fig. 7. We find that the GW spectra characterized by $f_{\text{peak}} = 10^{-9}$ Hz and $\Omega_{\text{GW}}^{\text{peak}} h^2 > \mathcal{O}(10^{-14})$ can explain the current PTA GW data and be confirmed by upcoming PTA such as SKA. As discussed above, although the peak amplitude of the GW spectra in scenario B can be significantly larger than that in scenario A, the former only marginally accounts for the diphoton and $b\bar{b}$ excesses at the 1σ level, whereas the latter can fully explain both excesses within the 1σ range.

VI. CONCLUSION

After imposing relevant theoretical and experimental constraints, we studied the diphoton and $b\bar{b}$ excesses at 95.4 GeV, along with the nano-Hertz GW signatures originating from

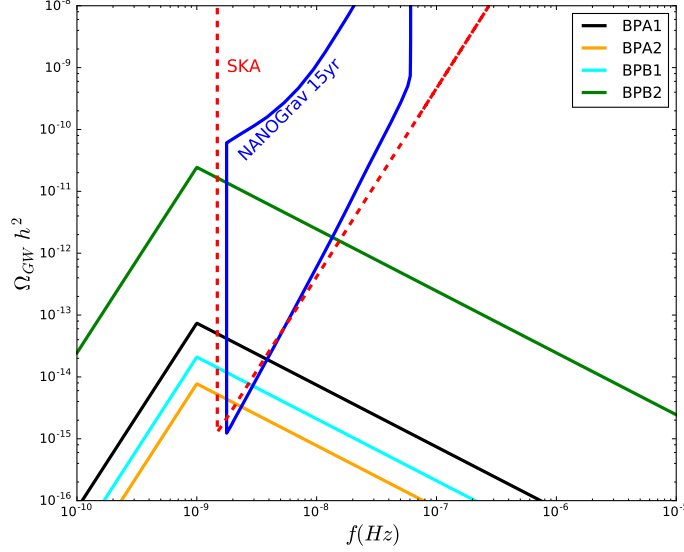


FIG. 7: The GW spectra $\Omega_{GW}h^2$ as a function of the frequency f . The result of the NANOGrav 15-year dataset [63, 64] and the sensitivity of SKA [150] are also displayed.

	$m_{h_3}(\text{GeV})$	$m_A = m_{H^\pm}(\text{GeV})$	$m_{12}^2(\text{GeV})^2$	$\tan \beta$	s_1	s_2	s_3
BPA1	455.71	623.58	35771.69	1.37	0.2875	0.9174	-0.7973
BPA2	441.82	549.95	28387.58	1.85	0.4013	0.9165	-0.7890
BPB1	3202.30	331.47	683.50	13.09	0.2108	0.0406	0.1644
BPB2	3349.33	431.49	649.92	14.76	0.2633	0.0260	0.0569

	$v_s(\text{GeV})$	λ_6	$\hat{\sigma}_{wall}$	\hat{V}_{bias}	$\Omega_{GW}^{peak} h^2$	χ_{95}^2
BPA1	44917.62	1.06×10^{-5}	128.05	36.97	7.39×10^{-14}	1.99
BPA2	24174.21	3.61×10^{-5}	41.45	11.97	7.75×10^{-15}	2.22
BPB1	5721.32	3.04×10^{-1}	68.20	19.69	2.10×10^{-14}	3.78
BPB2	32336.01	1.07×10^{-2}	2328.69	672.3	2.45×10^{-11}	2.42

TABLE I: Input parameters and results for the BPA1, BPA2, BPB1 and BPB2. Here $m_{h_1} = 95.4$ GeV and $m_{h_2} = 125.5$ GeV are fixed.

domain walls, within the framework of the N2HDM. When the 95.4 GeV Higgs boson predominantly originates from the singlet field, we found that the model fully accounts for the diphoton and $b\bar{b}$ excesses at 95.4 GeV within the 1σ range. Additionally, this scenario can predict a GW spectrum with a peak amplitude of 2×10^{-12} at a peak frequency of 10^{-9} Hz for $v_s = 100$ TeV. When the 95.4 GeV Higgs boson arises mainly from the CP-even

components of the Higgs doublets, we found that the scenario only marginally accounts for the diphoton and $b\bar{b}$ excesses at the 1σ level, but can yield a significantly enhanced GW amplitude of 6×10^{-8} at the same frequency for the same value of v_s . The nano-Hertz GW signals predicted by the model can explain the current PTA GW data and be confirmed by upcoming PTA such as SKA. The viable parameter space corresponding to each scenario have been explicitly mapped out. Our works highlight the complementary roles of collider signals and GW observables in probing the nature of the extended Higgs sector.

Acknowledgment

We thank Yang Zhang and Yeling Zhou for helpful discussions. This work was supported by the National Natural Science Foundation of China under Grant No. 11975013 and by the Projects No. ZR2024MA001 and No. ZR2023MA038 supported by Shandong Provincial Natural Science Foundation.

-
- [1] R. Barate *et al.* [LEP Working Group for Higgs boson searches, ALEPH, DELPHI, L3 and OPAL], Search for the standard model Higgs boson at LEP, *Phys. Lett. B* **565** (2003), 61-75.
 - [2] CMS collaboration, Search for a standard model-like Higgs boson in the mass range between 70 and 110 GeV in the diphoton final state in proton-proton collisions at $\sqrt{s} = 13$ TeV, CMS-PAS-HIG-20-002, 2023.
 - [3] G. Aad *et al.* [ATLAS], Search for diphoton resonances in the 66 to 110 GeV mass range using pp collisions at $\sqrt{s} = 13$ TeV with the ATLAS detector, *JHEP* **01** (2025), 053.
 - [4] T. Biekötter, S. Heinemeyer and G. Weiglein, 95.4 GeV diphoton excess at ATLAS and CMS, *Phys. Rev. D* **109** (2024), 3.
 - [5] J. Cao, X. Guo, Y. He, P. Wu and Y. Zhang, Diphoton signal of the light Higgs boson in natural NMSSM, *Phys. Rev. D* **95** (2017), 116001.
 - [6] T. Biekötter, M. Chakraborti and S. Heinemeyer, “A 96 GeV Higgs boson in the N2HDM,” *Eur. Phys. J. C* **80** (2020), 2.
 - [7] S. Heinemeyer, C. Li, F. Lika, G. Moortgat-Pick and S. Paasch, Phenomenology of a 96 GeV Higgs boson in the 2HDM with an additional singlet, *Phys. Rev. D* **106** (2022), 075003.

- [8] T. Biekötter, S. Heinemeyer and G. Weiglein, Mounting evidence for a 95 GeV Higgs boson, *JHEP* **08** (2022), 201.
- [9] J. A. Aguilar-Saavedra, H. B. Câmara, F. R. Joaquim and J. F. Seabra, Confronting the 95 GeV excesses within the U(1)-extended next-to-minimal 2HDM, *Phys. Rev. D* **108** (2023), 075020.
- [10] K. Choi, S. H. Im, K. S. Jeong and C. B. Park, Light Higgs bosons in the general NMSSM, *Eur. Phys. J. C* **79** (2019), 956.
- [11] S. Ma, K. Wang and J. Zhu, Higgs decay to light (pseudo)scalars in the semi-constrained NMSSM, *Chin. Phys. C* **45** (2021), 023113.
- [12] W. Li, H. Qiao and J. Zhu, Light Higgs boson in the NMSSM confronted with the CMS di-photon and di-tau excesses, *Chin. Phys. C* **47** (2023), 123102.
- [13] U. Ellwanger and C. Hugonie, Additional Higgs Bosons near 95 and 650 GeV in the NMSSM, *Eur. Phys. J. C* **83** (2023), 1138.
- [14] P. S. B. Dev, R. N. Mohapatra and Y. Zhang, Explanation of the 95 GeV $\gamma\gamma$ and $b\bar{b}$ excesses in the minimal left-right symmetric model, *Phys. Lett. B* **849** (2024), 138481.
- [15] C. Bonilla, A. E. Carcamo Hernandez, S. Kovalenko, H. Lee, R. Pasechnik and I. Schmidt, Fermion mass hierarchy in an extended left-right symmetric model, *JHEP* **12** (2023), 075.
- [16] C. X. Liu, Y. Zhou, X. Y. Zheng, J. Ma, T. F. Feng and H. B. Zhang, 95 GeV excess in a CP-violating μ -from- ν SSM, *Phys. Rev. D* **109** (2024), 056001.
- [17] W. Li, H. Qiao, K. Wang and J. Zhu, Light dark matter confronted with the 95 GeV diphoton excess, arXiv:2312.17599.
- [18] G. Abbas and N. Singh, Dark-technicolour at low scale, arXiv:2312.16532.
- [19] A. Ahriche, M. L. Bellilet, M. O. Khojali, M. Kumar and A. T. Mulaudzi, The scale invariant scotogenic model: CDF-II W -boson mass and the 95 GeV excesses, arXiv:2311.08297.
- [20] J. Cao, X. Jia, J. Lian and L. Meng, 95 GeV diphoton and $b\bar{b}$ excesses in the general next-to-minimal supersymmetric standard model, *Phys. Rev. D* **109** (2024), 075001.
- [21] M. Maniatis and O. Nachtmann, CMS results for the $\gamma\gamma$ production at the LHC: do they give a hint for a Higgs boson of the maximally CP symmetric two-Higgs-doublet model?, arXiv:2309.04869.
- [22] A. Belyaev, R. Benbrik, M. Boukidi, M. Chakraborti, S. Moretti and S. Semmlali, Explanation of the hints for a 95 GeV Higgs boson within a 2-Higgs Doublet Model, *JHEP* **05** (2024),

209.

- [23] D. Azevedo, T. Biekötter and P. M. Ferreira, 2HDM interpretations of the CMS diphoton excess at 95 GeV, *JHEP* **11** (2023), 017.
- [24] D. Bhatia, N. Desai and S. Dwivedi, Discovery prospects of a light charged Higgs near the fermiophobic region of Type-I 2HDM, *JHEP* **06** (2023), 100.
- [25] T. K. Chen, C. W. Chiang, S. Heinemeyer and G. Weiglein, 95 GeV Higgs boson in the Georgi-Machacek model, *Phys. Rev. D* **109** (2024), 075043.
- [26] A. Ahriche, The 95 GeV Excess in the Georgi-Machacek Model: Single or Twin Peak Resonance, arXiv:2312.10484.
- [27] G. Arcadi, G. Busoni, D. Cabo-Almeida and N. Krishnan, Is there a (Pseudo)Scalar at 95 GeV?, arXiv:2311.14486.
- [28] D. Borah, S. Mahapatra, P. K. Paul and N. Sahu, Scotogenic $U(1)_{L\mu-L\tau}$ origin of $(g-2)\mu$, W -mass anomaly and 95 GeV excess, *Phys. Rev. D* **109** (2024), 055021.
- [29] S. Banik, G. Coloretti, A. Crivellin and B. Mellado, Uncovering New Higgses in the LHC Analyses of Differential $t\bar{t}$ Cross Sections, arXiv:2308.07953.
- [30] J. Dutta, J. Lahiri, C. Li, G. Moortgat-Pick, S. F. Tabira and J. A. Ziegler, Dark Matter Phenomenology in 2HDMS in light of the 95 GeV excess, arXiv:2308.05653.
- [31] S. Bhattacharya, G. Coloretti, A. Crivellin, S. E. Dahbi, Y. Fang, M. Kumar and B. Mellado, Growing Excesses of New Scalars at the Electroweak Scale, arXiv:2306.17209.
- [32] S. Ashanujjaman, S. Banik, G. Coloretti, A. Crivellin, B. Mellado and A. T. Mulaudzi, $SU(2)_L$ triplet scalar as the origin of the 95 GeV excess?, *Phys. Rev. D* **108** (2023), L091704.
- [33] P. Escribano, V. M. Lozano and A. Vicente, Scotogenic explanation for the 95 GeV excesses, *Phys. Rev. D* **108** (2023), 115001.
- [34] T. Biekötter, S. Heinemeyer and G. Weiglein, The CMS di-photon excess at 95 GeV in view of the LHC Run 2 results, *Phys. Lett. B* **846** (2023), 138217.
- [35] S. Banik, A. Crivellin, S. Iguro and T. Kitahara, Asymmetric di-Higgs signals of the next-to-minimal 2HDM with a $U(1)$ symmetry, *Phys. Rev. D* **108** (2023), 075011.
- [36] G. Coloretti, A. Crivellin, S. Bhattacharya and B. Mellado, Searching for low-mass resonances decaying into W bosons, *Phys. Rev. D* **108** (2023), 035026.
- [37] A. Ahriche, Constraining the Georgi-Machacek model with a light Higgs boson, *Phys. Rev. D* **107** (2023), 015006.

- [38] R. Benbrik, M. Boukidi, S. Moretti and S. Semlali, Explaining the 96 GeV Di-photon anomaly in a generic 2HDM Type-III, *Phys. Lett. B* **832** (2022), 137245.
- [39] T. Biekötter, S. Heinemeyer and G. Weiglein, Excesses in the low-mass Higgs-boson search and the W -boson mass measurement, *Eur. Phys. J. C* **83** (2023), 450.
- [40] T. Biekötter, A. Grohsjean, S. Heinemeyer, C. Schwanenberger and G. Weiglein, Possible indications for new Higgs bosons in the reach of the LHC: N2HDM and NMSSM interpretations, *Eur. Phys. J. C* **82** (2022), 178.
- [41] A. A. Abdelalim, B. Das, S. Khalil and S. Moretti, Di-photon decay of a light Higgs state in the BLSSM, *Nucl. Phys. B* **985** (2022), 116013.
- [42] T. Biekötter, M. Chakraborti and S. Heinemeyer, The “96 GeV excess” at the LHC, *Int. J. Mod. Phys. A* **36** (2021), 2142018.
- [43] J. A. Aguilar-Saavedra and F. R. Joaquim, Multiphoton signals of a (96 GeV?) stealth boson, *Eur. Phys. J. C* **80** (2020), 403.
- [44] J. Cao, X. Jia, Y. Yue, H. Zhou and P. Zhu, 96 GeV diphoton excess in seesaw extensions of the natural NMSSM, *Phys. Rev. D* **101** (2020), 055008.
- [45] A. Kundu, S. Maharana and P. Mondal, A 96 GeV scalar tagged to dark matter models, *Nucl. Phys. B* **955** (2020), 115057.
- [46] J. Cao, X. Jia and J. Lian, Unified Interpretation of Muon $g-2$ anomaly, 95 GeV Diphoton, and $b\bar{b}$ Excesses in the General Next-to-Minimal Supersymmetric Standard Model, arXiv:2402.15847.
- [47] J. Kalinowski and W. Kotlarski, Interpreting 95 GeV di-photon/ $b\bar{b}$ excesses as a lightest Higgs boson of the MRSSM, *JHEP* **07** (2024), 037.
- [48] U. Ellwanger, C. Hugonie, S. F. King and S. Moretti, NMSSM Explanation for Excesses in the Search for Neutralinos and Charginos and a 95 GeV Higgs Boson, arXiv:2404.19338.
- [49] R. Benbrik, M. Boukidi and S. Moretti, Superposition of CP-Even and CP-Odd Higgs Resonances: Explaining the 95 GeV Excesses within a Two-Higgs Doublet Model, arXiv:2405.02899.
- [50] J. Lian, The 95GeV Excesses in the \mathbb{Z}_3 -symmetric Next-to Minimal Supersymmetric Standard Model, arXiv:2406.10969.
- [51] J. L. Yang, M. H. Guo, W. H. Zhang, H. B. Zhang and T. F. Feng, Explaining the possible 95 GeV excesses in the $B - L$ symmetric SSM, arXiv:2406.01926.

- [52] P. Janot, The infamous 95 GeV $b\bar{b}$ excess at LEP: Two b or not two b?, arXiv:2407.10948.
- [53] J. Gao, X. F. Han, J. Ma, L. Wang and H. Xu, 95 GeV Higgs boson and spontaneous CP-violation at the finite temperature, Phys. Rev. D **110** (2024), 115045.
- [54] A. Khanna, S. Moretti and A. Sarkar, Explaining 95 (or so) GeV Anomalies in the 2-Higgs Doublet Model Type-I, arXiv:2409.02587.
- [55] B. Ait-Ouazghour, M. Chabab and K. Goure, Unified Interpretation of 95 GeV Excesses in the Two Higgs Doublet type II Seesaw Model, arXiv:2410.11140.
- [56] S. Gao, S. M. Zhao, S. Di, X. X. Dong and T. F. Feng, A 95 GeV Higgs Boson in the $U(1)_X$ model, arXiv:2411.13261.
- [57] T. Mondal, S. Moretti and P. Sanyal, On the CP Nature of the ‘95 GeV’ Anomalies, arXiv:2412.00474.
- [58] S. Banik, G. Coloretti, A. Crivellin and H. E. Haber, Correlating $A \rightarrow \gamma\gamma$ with electric dipole moments in the two Higgs doublet model in light of the diphoton excesses at 95 GeV and 152 GeV, Phys. Rev. D **111** (2025), 075021.
- [59] A. Hmissou, S. Moretti and L. Rahili, Investigating the 95 GeV Higgs Boson Excesses within the I(1+2)HDM, arXiv:2502.03631.
- [60] X. Du, H. Liu and Q. Chang, Interpretation of 95 GeV Excess within the Georgi-Machacek Model in Light of Positive Definiteness Constraints, arXiv:2502.06444.
- [61] A. Arhrib, K. H. Phan, V. Q. Tran and T. C. Yuan, When the Standard Model Higgs meets its lighter 95 GeV twin, Nucl. Phys. B **1015** (2025), 116909.
- [62] Z. Li, N. Liu and B. Zhu, Interplay of 95 GeV Diphoton Excess and Dark Matter in Supersymmetric Triplet Model, arXiv:2504.21273.
- [63] G. Agazie *et al.* [NANOGrav], The NANOGrav 15 yr Data Set: Evidence for a Gravitational-wave Background, Astrophys. J. Lett. **951** (2023), L8.
- [64] G. Agazie *et al.* [NANOGrav], The NANOGrav 15 yr Data Set: Constraints on Supermassive Black Hole Binaries from the Gravitational-wave Background, Astrophys. J. Lett. **952** (2023), L37.
- [65] J. Antoniadis *et al.* [EPTA], The second data release from the European Pulsar Timing Array - I. The dataset and timing analysis, Astron. Astrophys. **678** (2023), A48.
- [66] J. Antoniadis *et al.* [EPTA and InPTA], The second data release from the European Pulsar Timing Array - II. Customised pulsar noise models for spatially correlated gravitational

- waves, *Astron. Astrophys.* **678** (2023), A49.
- [67] D. J. Reardon, A. Zic, R. M. Shannon, G. B. Hobbs, M. Bailes, V. Di Marco, A. Kapur, A. F. Rogers, E. Thrane and J. Askew, *et al.* Search for an Isotropic Gravitational-wave Background with the Parkes Pulsar Timing Array, *Astrophys. J. Lett.* **951** (2023), L6.
- [68] H. Xu, S. Chen, Y. Guo, J. Jiang, B. Wang, J. Xu, Z. Xue, R. N. Caballero, J. Yuan and Y. Xu, *et al.* Searching for the Nano-Hertz Stochastic Gravitational Wave Background with the Chinese Pulsar Timing Array Data Release I, *Res. Astron. Astrophys.* **23** (2023), 075024.
- [69] A. Afzal *et al.* [NANOGrav], “The NANOGrav 15 yr Data Set: Search for Signals from New Physics,” *Astrophys. J. Lett.* **951** (2023), L11 [erratum: *Astrophys. J. Lett.* **971** (2024) , L27; erratum: *Astrophys. J.* **971** (2024) , L27].
- [70] J. Ellis, M. Lewicki, C. Lin and V. Vaskonen, Cosmic superstrings revisited in light of NANOGrav 15-year data, *Phys. Rev. D* **108** (2023), 103511.
- [71] L. Bian, S. Ge, J. Shu, B. Wang, X. Y. Yang and J. Zong, Gravitational wave sources for pulsar timing arrays, *Phys. Rev. D* **109** (2024), L101301.
- [72] Z. Wang, L. Lei, H. Jiao, L. Feng and Y.-Z. Fan, The nanohertz stochastic gravitational wave background from cosmic string loops and the abundant high redshift massive galaxies, *Sci. China Phys. Mech. Astron.* **66** (2023), 120403.
- [73] G. Lazarides, R. Maji and Q. Shafi, Superheavy quasistable strings and walls bounded by strings in the light of NANOGrav 15 year data, *Phys. Rev. D* **108** (2023), 095041.
- [74] A. Eichhorn, R. R. Lino dos Santos and J. a. L. Miqueleto, From quantum gravity to gravitational waves through cosmic strings, *Phys. Rev. D* **109** (2024), 026013.
- [75] D. Chowdhury, G. Tasinato and I. Zavala, Dark energy, D-branes and pulsar timing arrays, *JCAP* **11** (2023), 090.
- [76] S. Antusch, K. Hinze, S. Saad and J. Steiner, Singling out SO(10) GUT models using recent PTA results, *Phys. Rev. D* **108** (2023), 095053.
- [77] M. Yamada and K. Yonekura, Dark baryon from pure Yang-Mills theory and its GW signature from cosmic strings, *JHEP* **09** (2023), 197.
- [78] S. Ge, Stochastic gravitational wave background: birth from string-wall death, *JCAP* **06** (2024), 064.
- [79] S. Basilakos, D. V. Nanopoulos, T. Papanikolaou, E. N. Saridakis and C. Tzerefos, Gravitational wave signatures of no-scale supergravity in NANOGrav and beyond, *Phys. Lett. B*

- 850** (2024), 138507.
- [80] A. Avgoustidis, E. J. Copeland, A. Moss and J. Raidal, The stochastic gravitational wave background from cosmic superstrings, arXiv:2503.10361.
- [81] N. Kitajima, J. Lee, K. Murai, F. Takahashi and W. Yin, Gravitational waves from domain wall collapse, and application to nanohertz signals with QCD-coupled axions, Phys. Lett. B **851** (2024), 138586.
- [82] S. Blasi, A. Mariotti, A. Rase and A. Sevrin, Axionic domain walls at Pulsar Timing Arrays: QCD bias and particle friction, JHEP **11** (2023), 169.
- [83] Y. Gouttenoire and E. Vitagliano, Domain wall interpretation of the PTA signal confronting black hole overproduction, Phys. Rev. D **110** (2024), L061306.
- [84] B.-Q. Lu, C.-W. Chiang and T. Li, Clockwork axion footprint on nanohertz stochastic gravitational wave background, Phys. Rev. D **109** (2024), L101304.
- [85] E. Babichev, D. Gorbunov, S. Ramazanov, R. Samanta and A. Vikman, NANOGrav spectral index $\gamma = 3$ from melting domain walls, Phys. Rev. D **108** (2023), 123529.
- [86] G. B. Gelmini and J. Hyman, Catastrogenesis with unstable ALPs as the origin of the NANOGrav 15 yr gravitational wave signal, Phys. Lett. B **848** (2024), 138356.
- [87] S.-Y. Guo, M. Khlopov, X. Liu, L. Wu, Y. Wu and B. Zhu, Footprints of axion-like particle in pulsar timing array data and James Webb Space Telescope observations, Sci. China Phys. Mech. Astron. **67** (2024), 111011.
- [88] Z. Zhang, C. Cai, Y.-H. Su, S. Wang, Z.-H. Yu and H.-H. Zhang, Nano-Hertz gravitational waves from collapsing domain walls associated with freeze-in dark matter in light of pulsar timing array observations, Phys. Rev. D **108** (2023), 095037.
- [89] M. X. Huang, F. Wang and Y. K. Zhang, Interplay between the muon $g-2$ anomaly and the PTA nHZ gravitational waves from domain walls in the next-to-minimal supersymmetric standard model, Phys. Rev. D **109** (2024), 075032.
- [90] X. K. Du, M. X. Huang, F. Wang and Y. K. Zhang, Did the nHZ Gravitational Waves Signatures Observed By NANOGrav Indicate Multiple Sector SUSY Breaking?, arXiv:2307.02938.
- [91] H. J. Li and Y. F. Zhou, Gravitational waves and primordial black holes from axion domain walls in level crossing*, Chin. Phys. C **49** (2025), 035101.
- [92] Y. Li, L. Bian, R. G. Cai and J. Shu, Cosmic Simulations of Axion String-Wall Networks: Probing Dark Matter and Gravitational Waves for Discovery, arXiv:2311.02011.

- [93] B. Q. Lu, C. W. Chiang and T. Li, A Common Origin for Nano-Hz Gravitational Wave Background and Black Hole Merger Events, arXiv:2409.10251.
- [94] K. Fujikura, S. Girmohanta, Y. Nakai and M. Suzuki, NANOGrav signal from a dark conformal phase transition, *Phys. Lett. B* **846** (2023), 138203.
- [95] G. Franciolini, D. Racco and F. Rompineve, Footprints of the QCD Crossover on Cosmological Gravitational Waves at Pulsar Timing Arrays, *Phys. Rev. Lett.* **132** (2024), 081001.
- [96] T. Bringmann, P. F. Depta, T. Konstandin, K. Schmidt-Hoberg and C. Tasillo, Does NANOGrav observe a dark sector phase transition?, *JCAP* **11** (2023), 053.
- [97] A. Addazi, Y.-F. Cai, A. Marciano and L. Visinelli, Have pulsar timing array methods detected a cosmological phase transition?, *Phys. Rev. D* **109** (2024), 015028.
- [98] Y. Bai, T.-K. Chen and M. Korwar, QCD-collapsed domain walls: QCD phase transition and gravitational wave spectroscopy, *JHEP* **12** (2023), 194.
- [99] C. Han, K.-P. Xie, J. M. Yang and M. Zhang, Self-interacting dark matter implied by nano-Hertz gravitational waves, *Phys. Rev. D* **109** (2024), 115025.
- [100] L. Zu, C. Zhang, Y.-Y. Li, Y. Gu, Y.-L. S. Tsai and Y.-Z. Fan, Mirror QCD phase transition as the origin of the nanohertz Stochastic Gravitational-Wave Background, *Sci. Bull.* **69** (2024), 741–746.
- [101] T. Ghosh, A. Ghoshal, H.-K. Guo, F. Hajkarim, S. F. King, K. Sinha et al., Did we hear the sound of the Universe boiling? Analysis using the full fluid velocity profiles and NANOGrav 15-year data, *JCAP* **05** (2024), 100.
- [102] Y. Xiao, J. M. Yang and Y. Zhang, Implications of nano-Hertz gravitational waves on electroweak phase transition in the singlet dark matter model, *Sci. Bull.* **68** (2023), 3158–3164.
- [103] S.-P. Li and K.-P. Xie, Collider test of nano-Hertz gravitational waves from pulsar timing arrays, *Phys. Rev. D* **108** (2023), 055018.
- [104] P. Di Bari and M. H. Rahat, Split Majoron model confronts the NANOGrav signal and cosmological tensions, *Phys. Rev. D* **110** (2024), 055019.
- [105] J. S. Cruz, F. Niedermann and M. S. Sloth, NANOGrav meets Hot New Early Dark Energy and the origin of neutrino mass, *Phys. Lett. B* **846** (2023), 138202.
- [106] Y. Gouttenoire, First-Order Phase Transition Interpretation of Pulsar Timing Array Signal Is Consistent with Solar-Mass Black Holes, *Phys. Rev. Lett.* **131** (2023), 171404.
- [107] M. Ahmadvand, L. Bian and S. Shakeri, Heavy QCD axion model in light of pulsar timing

- arrays, *Phys. Rev. D* **108** (2023), 115020.
- [108] A. Salvio, Supercooling in radiative symmetry breaking: theory extensions, gravitational wave detection and primordial black holes, *JCAP* **12** (2023), 046.
- [109] P. Athron, A. Fowlie, C. T. Lu, L. Morris, L. Wu, Y. Wu and Z. Xu, Can Supercooled Phase Transitions Explain the Gravitational Wave Background Observed by Pulsar Timing Arrays?, *Phys. Rev. Lett.* **132** (2024), 221001.
- [110] S. Jiang, A. Yang, J. Ma and F. P. Huang, Implication of nano-Hertz stochastic gravitational wave on dynamical dark matter through a dark first-order phase transition, *Class. Quant. Grav.* **41** (2024), 065009.
- [111] S. He, L. Li, S. Wang and S. J. Wang, Constraints on holographic QCD phase transitions from PTA observations, *Sci. China Phys. Mech. Astron.* **68** (2025), 210411.
- [112] W. Chao, J. J. Feng, H. K. Guo and T. Li, Oscillations of ultralight dark photon into gravitational waves, *Nucl. Phys. B* **1009** (2024), 116740.
- [113] J. Gonçalves, D. Marfatia, A. P. Morais and R. Pasechnik, Supercooled phase transitions in conformal dark sectors explain NANOGrav data, arXiv:2501.11619.
- [114] F. Costa, J. Hoefken Zink, M. Lucente, S. Pascoli and S. Rosauero-Alcaraz, Supercooled Dark Scalar Phase Transitions explanation of NANOGrav data, arXiv:2501.15649.
- [115] S. Vagnozzi, Inflationary interpretation of the stochastic gravitational wave background signal detected by pulsar timing array experiments, *JHEAp* **39** (2023), 81–98.
- [116] L. Frosina and A. Urbano, Inflationary interpretation of the nHz gravitational-wave background, *Phys. Rev. D* **108** (2023), 103544.
- [117] L. Liu, Z.-C. Chen and Q.-G. Huang, Implications for the non-Gaussianity of curvature perturbation from pulsar timing arrays, *Phys. Rev. D* **109** (2024), L061301.
- [118] C. Unal, A. Papageorgiou and I. Obata, Axion-gauge dynamics during inflation as the origin of pulsar timing array signals and primordial black holes, *Phys. Lett. B* **856** (2024), 138873.
- [119] P. Bari, N. Bartolo, G. Domenech and S. Matarrese, Gravitational waves induced by scalar-tensor mixing, *Phys. Rev. D* **109** (2024), 023509.
- [120] B. Das, N. Jaman and M. Sami, Gravitational wave background from quintessential inflation and NANOGrav data, *Phys. Rev. D* **108** (2023), 103510.
- [121] J.-Q. Jiang, Y. Cai, G. Ye and Y.-S. Piao, Broken blue-tilted inflationary gravitational waves: a joint analysis of NANOGrav 15-year and BICEP/Keck 2018 data, *JCAP* **05** (2024), 004.

- [122] M. A. Gorji, M. Sasaki and T. Suyama, Extra-tensor-induced origin for the PTA signal: No primordial black hole production, *Phys. Lett. B* **846** (2023), 138214.
- [123] H. An, B. Su, H. Tai, L. T. Wang and C. Yang, Phase transition during inflation and the gravitational wave signal at pulsar timing arrays, *Phys. Rev. D* **109** (2024), L121304.
- [124] J. Cang, Y. Gao, Y. Liu and S. Sun, Implications of pulsar timing array results for high frequency gravitational waves, *Phys. Lett. B* **864** (2025), 139429.
- [125] C. Y. Chen, M. Freid and M. Sher, Next-to-minimal two Higgs doublet model, *Phys. Rev. D* **89** (2014), 075009.
- [126] M. Muhlleitner, M. O. P. Sampaio, R. Santos and J. Wittbrodt, The N2HDM under Theoretical and Experimental Scrutiny, *JHEP* **03** (2017), 094.
- [127] I. Engeln, M. Mühlleitner and J. Wittbrodt, N2HDECAY: Higgs Boson Decays in the Different Phases of the N2HDM, *Comput. Phys. Commun.* **234** (2019), 256-262.
- [128] M. Y. Sassi and G. Moortgat-Pick, Electroweak Symmetry Restoration in the N2HDM via Domain Walls, arXiv:2407.14468.
- [129] A. Vilenkin, Gravitational Field of Vacuum Domain Walls and Strings, *Phys. Rev. D* **23** (1981), 852-857.
- [130] G. B. Gelmini, M. Gleiser and E. W. Kolb, Cosmology of Biased Discrete Symmetry Breaking, *Phys. Rev. D* **39** (1989), 1558.
- [131] S. E. Larsson, S. Sarkar and P. L. White, Evading the cosmological domain wall problem, *Phys. Rev. D* **55** (1997), 5129-5135.
- [132] L. Wang, J. M. Yang and Y. Zhang, Two-Higgs-doublet models in light of current experiments: a brief review, *Commun. Theor. Phys.* **74** (2022), 097202.
- [133] H. Bahl, T. Biekötter, S. Heinemeyer, C. Li, S. Paasch, G. Weiglein and J. Wittbrodt, HiggsTools: BSM scalar phenomenology with new versions of HiggsBounds and HiggsSignals, *Comput. Phys. Commun.* **291** (2023), 108803.
- [134] P. Bechtle, S. Heinemeyer, O. Stål, T. Stefaniak and G. Weiglein, *HiggsSignals*: Confronting arbitrary Higgs sectors with measurements at the Tevatron and the LHC, *Eur. Phys. J. C* **74** (2014), 2711.
- [135] P. Bechtle, D. Dercks, S. Heinemeyer, T. Klingl, T. Stefaniak, G. Weiglein and J. Wittbrodt, HiggsBounds-5: Testing Higgs Sectors in the LHC 13 TeV Era, *Eur. Phys. J. C* **80** (2020), 1211.

- [136] P. Bechtle, O. Brein, S. Heinemeyer, G. Weiglein and K. E. Williams, HiggsBounds: Confronting Arbitrary Higgs Sectors with Exclusion Bounds from LEP and the Tevatron, *Comput. Phys. Commun.* **181** (2010), 138-167.
- [137] F. Mahmoudi, SuperIso v2.3: A Program for calculating flavor physics observables in Supersymmetry, *Comput. Phys. Commun.* **180** (2009), 1579-1613.
- [138] P. A. Zyla et al. [Particle Data Group], Review of Particle Physics, *PTEP* **2020**, 083C01 (2020).
- [139] H.-J. He, N. Polonsky, S. Su, Extra families, Higgs spectrum and oblique corrections, *Phys. Rev. D* **64** (2001), 053004.
- [140] H. E. Haber, D. O'Neil, Basis-independent methods for the two-Higgs-doublet model. III. The CP-conserving limit, custodial symmetry, and the oblique parameters S, T, U, *Phys. Rev. D* **83** (2011), 055017.
- [141] A. Djouadi, The Anatomy of electro-weak symmetry breaking. II. The Higgs bosons in the minimal supersymmetric model, *Phys. Rept.* **459** (2008), 1-241.
- [142] H. Hattori, T. Kobayashi, N. Omoto and O. Seto, Entropy production by domain wall decay in the NMSSM, *Phys. Rev. D* **92** (2015), 103518.
- [143] C. L. Wainwright, CosmoTransitions: Computing Cosmological Phase Transition Temperatures and Bubble Profiles with Multiple Fields, *Computl. Phys. Commun.* **183** (2012), 2006-2013.
- [144] N. Chen, T. Li and Y. Wu, The gravitational waves from the collapsing domain walls in the complex singlet model, *JHEP* **08** (2020), 117.
- [145] T. Hiramatsu, M. Kawasaki and K. Saikawa, On the estimation of gravitational wave spectrum from cosmic domain walls, *JCAP* **02** (2014), 031.
- [146] K. Saikawa, A review of gravitational waves from cosmic domain walls, *Universe* **3** (2017), 40.
- [147] M. Kawasaki, K. Kohri and T. Moroi, Big-Bang nucleosynthesis and hadronic decay of long-lived massive particles, *Phys. Rev. D* **71** (2005), 083502.
- [148] L. Husdal, On Effective Degrees of Freedom in the Early Universe, *Galaxies* **4** (2016), 78.
- [149] T. Hiramatsu, M. Kawasaki and K. Saikawa, Gravitational Waves from Collapsing Domain Walls, *JCAP* **05** (2010), 032.
- [150] C. L. Carilli and S. Rawlings, Science with the Square Kilometer Array: Motivation, key

science projects, standards and assumptions, *New Astron. Rev.* **48** (2004), 979.